© Universiti Tun Hussein Onn Malaysia Publisher's Office

JAMEA

http://penerbit.uthm.edu.my/ojs/index.php/jamea

e-ISSN : 2716-6201

Journal of Advanced Mechanical Engineering Applications

Comparative Study of Two Dimensional Boundary Layer over NACA 23012 and NACA 23021 Airfoils by Using Keller's Box Method

Vinod Kumar K Sivak Kumar[1], Aslam Abdullah[1]*, Bambang Basuno[1]

[1]Faculty of Mechanical and Manufacturing Engineering,
Universiti Tun Hussein Onn Malaysia, Batu Pahat, 86400, MALAYSIA

*Corresponding Author

DOI: https://doi.org/10.30880/jamea.2022.03.01.004
Received 24 April 2022; Accepted 13 June 2022; Available online 20 July 2022

Abstract: This paper begins with general description on various methods for solving boundary layer equation. In particular, Prandtl's boundary layer equation is a simplified version of Navier-Stokes equation that is solved integrally. Order of magnitude analysis can be used to solve laminar and turbulent flow problems along the boundary layer. A more complex technique based on Keller's box method is also discussed. This study aims at utilising a developed computer code which allows one to predict the development of boundary layer characteristics along airfoils' surface, and have a comparative understanding on flow behaviours between NACA 23012 and NACA 23021 airfoils, as well as 0º and 5º angles of attack. The ability of Keller's box method to solve the boundary layer equation prevails through correct skin friction, momentum thickness, and shape factor distributions over the surfaces. It was found that skin friction in boundary layer over NACA 23021 is higher than that over NACA 23012 for about 10% of the chord length from the leading edge. However, momentum thickness of the boundary layer over NACA 23021 is less than the boundary layer momentum thickness over NACA 23012 for the whole chord length. Similarly, the shape factor *H* for the boundary layer over the former is smaller in comparison to the latter for about 30% of the chord length.

Keywords: Boundary layer, Keller's box method

1. Introduction

Ludwig Prandtl was a professor of mechanics in a mechanical engineering department, and had no interest in fluid mechanics before 1900. However, in 1904 he released his study "On the Motion of Fluids with Very Little Friction". It was only eight pages long, yet would prove to be one of the most important and prestige fluid-dynamics papers ever written. By 1930, Prandtl was recognized worldwide as the elder statesman of fluid dynamics [1].

He studied the influence of viscous effects on flow behaviors inside a limited domain, or boundary layer close to the body surface in high Reynolds number flow. The fluid motion governing equation, namely the Navier-Stokes partial differential equation, was applied to the flow inside the boundary layer, and simplified into a new equation called Ludwig Prandtl's boundary layer equation. Solving the equation inside the boundary layer requires a numerical method. A common numerical scheme used to solve the governing equation is called Keller's box method. The Keller's box method program code by Bradshaw [1, 2] will be adopted and used in this study to predict NACA 23012 and NACA 23021 aerodynamic properties, as well as those at two angles of attack (i.e. at $\alpha = 0^{\circ}$, and $\alpha = 5^{\circ}$).

*Corresponding author: aslam@uthm.edu.my

1.1 The Navier-Stokes Equation

The essential equations that describe a Newtonian flow are the continuity equation and the Navier-Stokes equations. However, there are assumptions that can be made if the flow obeys the laws of a Newtonian fluid [3];

- There is a linear relationship between the stress tensor and the rate of deformation.
- The fluid is isotropic and thus there is no locally preferred direction.
- In the hydrostatic stress state, all tangential forces vanish and thus tensor, $\tau^* = 0$.

The Continuity Equation for a two-dimensional incompressible flow is given as

$$\frac{\partial u^*}{\partial x^*} + \frac{\partial v}{\partial y^*} = 0 \tag{1}$$

and the Navier-Stokes equations for a two-dimensional incompressible flow is given as

$$\begin{aligned} \rho^*\left(\frac{\partial u^*}{\partial t^*} + u^*\frac{\partial u^*}{\partial x^*} + v^*\frac{\partial u^*}{\partial y^*} + w^*\frac{\partial u^*}{\partial z^*}\right) &= -\frac{\partial p^*}{\partial x^*} + \mu^*\left(\frac{\partial^2 u^*}{\partial x^{*2}} + \frac{\partial^2 u^*}{\partial y^{*2}}\right) \\ \rho^*\left(\frac{\partial v^*}{\partial t^*} + u^*\frac{\partial v^*}{\partial x^*} + v^*\frac{\partial v^*}{\partial y^*} + w^*\frac{\partial v^*}{\partial z^*}\right) &= -\frac{\partial p^*}{\partial y^*} + \mu^*\left(\frac{\partial^2 v^*}{\partial x^{*2}} + \frac{\partial^2 v}{\partial y^{*2}}\right) \end{aligned} \tag{2}$$

1.2 Derivation of the Boundary-Layer Equations

The boundary layer equations are simplified by using Equation 1 and the Navier-Stokes equations for a two-dimensional incompressible flow (i.e. Equation 2). As a result of Prandtl's boundary-layer concept in 1904, Prandtl clarified the role of viscosity in fluid flow that is dominant only in a tiny layer. By estimating the order of magnitude in each term in Equation 1 and 2, Prandtl obtain dimensionless equations for distance, *x* and *y*, velocity, *u*, speed, *v*, and pressure, *p* [1 - 3].

Studying each fraction of *x*, *y*, *u*, *v*, and *p* demonstrates that *x* and *u* are in magnitude order $\theta(1)$, the wall-normal distance *y* and speed *v* are in magnitude order $\theta(\delta^*)$. Upon applying the transformations of Equation 1 and 2, the magnitude of order $\theta(\delta)$ or less can be eliminated because δ in boundary layer should be small and as the Reynolds number approaches infinity. Thus, Equation 1 and 2 are reduced to a dimensionless form.

The momentum equation then implies that the pressure distribution is only *x* dependent. The pressure distribution can be taken from the boundary layer's edge because it is constant in *y*-direction. At the boundary layer's edge, viscous effects vanish, allowing potential solutions to calculate the pressure distribution. This implies that the velocity at the boundary layer's edge can be calculated directly by solving the momentum equation in streamwise direction. Thus the boundary-layer equations in physical coordinates for a steady, two-dimensional, incompressible flow is found. This equation reduces the number of variables from (*u*, *v*, *p*) to (*u*, *v*). The initial Navier-Stokes equations (i.e. Equation 2) also become parabolic, losing their elliptical nature. That is, the solution's effects only act downstream of the flow, greatly simplifying the equations. The boundary layer equations can be solved steadily. It is written as

$$\frac{\partial u^*}{\partial x^*} + \frac{\partial v^*}{\partial y^*} = 0 \tag{3}$$

$$u^*\frac{\partial u^*}{\partial x^*} + v^*\frac{\partial u^*}{\partial y^*} = -\frac{1}{\rho^*}\frac{\partial p^*}{\partial x^*} + v^*\frac{\partial^2 u^*}{\partial y^{*2}} \tag{4}$$

with

$$-\frac{1}{\rho^*}\frac{\partial p^*}{\partial x^*} = U_e^*\frac{\partial U_e^*}{\partial x^*} \tag{5}$$

and the boundary conditions

$$\begin{aligned} y^* = 0: \quad u^* = 0 \quad \text{and} \quad v^* = 0 \\ y^* \to \infty: \quad u^* = U_e^*(x) \end{aligned} \tag{6}$$

1.3 Integral Boundary-Layer Equation

The boundary-layer equation (i.e. Equation 4) is simplified if no velocity profiles are required. It is then solved for the integral boundary-layer quantities. The first applications of the momentum integral equation to the solution of the boundary layer were by Pohlhausen and Von Karman [4] who is also the former student of Prandtl's. From the first integral, Von Karman discovered that in an inviscid solution, the displacement thickness δ_1^* must be added to the airfoil

and from the second integral, he discovered the momentum thickness δ_2^*. The length of the airfoil needed to match an inviscid flow's total momentum thickness. It is defined as

$$\delta_2^* = \int_0^\infty \left[\frac{u^*}{U_e^*}\left(1 - \frac{u^*}{U_e^*}\right)\right] dy^* \tag{7}$$

By integrating Equation 4, the local shear stress, $\tau_w^*(x)$ at the wall can be analysed. Further simplification to the integral boundary-layer equation is generated upon including the displacement thickness δ_1^* and the momentum thickness δ_2^* which yields an integral equation of two-dimensional incompressible boundary-layer (i.e. Equation 8). Aside from that, solving Equation 8 yields another important boundary-layer feature that is the local skin friction coefficient, C_f (9).

$$\frac{\partial}{\partial x^*}\left(U_e^{*2}\delta_2^*\right) + \delta_1^* U_e^* \frac{dU_e^*}{dx^*} = \frac{\tau_w^*}{\rho^*} \quad \text{or} \quad \frac{d\delta_2^*}{dx^*} + \frac{2\delta_2^* + \delta_1^*}{U_e^*}\frac{dU_e^*}{dx^*} = \frac{\tau_w^*}{\rho^* U_e^{*2}} \tag{8}$$

$$C_f(x) = \frac{\tau_w^*(x)}{\frac{1}{2}\rho^* {U_\infty^*}^2} \tag{9}$$

1.3.1 Solutions of the Integral Boundary-Layer Equation

Since Equation 8 is an ordinary differential equation, it is easier to solve than the original boundary-layer equation (i.e. Equation 4). Historically, the integral boundary-layer equation was used to identify boundary layer characteristics because it could be solved quickly. The direct boundary-layer equation (i.e. Equation 4) can now be solved in a reasonable amount of time due to the increase in computing power over the last two decades [5 - 7]. It is worth noting that the integral boundary-layer equation is still used in turbulent flows for parameter studies and airfoil design programmes. The solutions discussed here are based on the First Walz method and Thwaites' method.

1.3.1.1 First Walz Method

This method uses the dimensionless boundary-layer profiles $\delta^*$and the more precise and specified momentum thickness δ_2^* to generate an alternative shape parameter λ from Equation 8. By introducing dimensionless parameter Z^*, the integral boundary-layer equation (i.e. Equation 8) becomes $U_e^*\delta_2^*/v$, which can be simplified with the definition of Z^*. Using the dimensionless pressure gradient Λ from Pohlhausen parameters [4], the function $F(\lambda)$ is now based on the momentum thickness.

With the Pohlhausen approach, the initial value $\lambda_0 = 0.0770$ is obtained. The second derivative of the edge velocity is eliminated when using momentum thickness results instead of boundary-layer thickness data. Next, the first derivative is used to calculate $Z^*(x^*)$ and the almost linear function $F(\lambda)$ is used to simplify the nonlinear differential equation. This linearization produces a closed-form solution that can be used to compute boundary-layer properties immediately

$$U_e^* Z^* = \frac{a}{U_e^{*b-1}} \int_0^{x^*} U_e^{*b-1} dx^* \tag{10}$$

1.3.1.2 Thwaites Method

Like the first Walz technique, Thwaites defined his method's shape parameter λ using the momentum thickness as well. A dimensionless parameter G is also introduced as specified in the first Walz technique and is used to solve the integral boundary-layer equation (i.e. Equation 8). Thwaites assumed the right-hand side of his final arrangement a universal function dependent on linear function $F(\lambda)$ [4]. Upon simplifying, it is then multiplied with dimensionless form velocity distribution U_e^* directly, transforming the equation to be solvable to obtain the dimensionless momentum thickness, δ_2^* for the well-known function as

$$\delta_2^2(x) = \delta_2^2(0)\left(\frac{U_e(0)}{U_e(x)}\right)^6 + \frac{0.45}{Re {U_e}^6(x)} \int_0^x {U_e}^5(x) dx \tag{11}$$

In order to describe a stagnation-point flow, Cebeci defined the dimensionless stagnation point's momentum thickness, $\delta_2^2(0)$ [8]. After obtaining $\delta_2(x)$, it is possible to determine the pressure gradient parameter Λ. Following that, the dimensionless skin friction parameter l and the shape factor $H_{12} = \frac{\delta_1}{\delta_2}$ are determined using the following relations

$$G(\lambda) \approx \begin{cases} 0.22 + 1.402\lambda + \dfrac{0.018\lambda}{0.107 + \lambda}, & for -0.1 \leq \lambda \leq 0 \\ 0.22 + 1.57\lambda - 1.8\lambda^2, & for\ 0 \leq \lambda \leq 0.1 \end{cases} \tag{12}$$

$$H_{12}(\lambda) \approx \begin{cases} 2.088 + \dfrac{0.0731}{0.14 + \lambda}, & \text{for} -0.1 \leq \lambda \leq 0 \\ 2.61 - 3.75\lambda + 5.24\lambda^2, & \text{for } 0 \leq \lambda \leq 0.1 \end{cases} \tag{13}$$

1.4 Transformation of the Boundary-Layer Equation

Since Equation 4 is still in partial differential equation, the direct boundary-layer equation is simplified numerically. To simplify flows near walls, the boundary-layer equation (i.e. Equation 4) is used. Falkner and Skan implemented that a suitable transformation can help simplify the answer, where the wall-normal scaling factor is introduced. The wall-normal quantity y is thus stretched to match the streamwise direction. As shown in Fig. 1(a), the maximum value of y increases streamwise as the boundary-layer thickness increases. The calculation domain must be expanded in the wall-normal way to satisfy the free-stream as in Equation 6. As shown in Fig. 1(b), boundary scaling in the wall-normal direction in Equation 12 prevents the computational domain from rising.

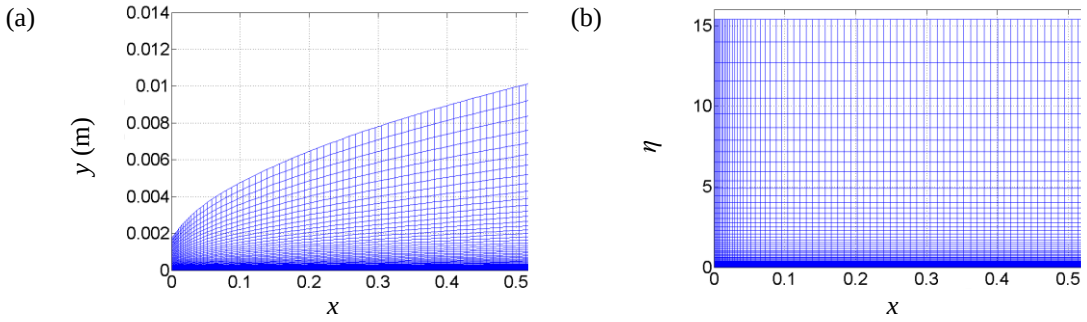

Fig. 1 - (a) Physical domain; (b) Dimensionless domain [9]

Introducing a dimensionless stream function, f that depends on x and η that solves the continuity equation (i.e. Equation 9), and adding the stream function f to the boundary layer equation, a set of derivatives need to be solved.

This boundary layer transformation can solve the boundary layer of any shape body, like an airfoil. Decomposition of the system of partial differential equations into a system of ordinary differential equations simplifies the solution. Remarkably, the solution can also be used for wedge flow, with a constant pressure gradient. Upon applying the Falkner-Skan transformation to the displacement thickness, δ_1 and momentum thickness, δ_2^* from Equation 7, it yields

$$\delta_2^* = \sqrt{\frac{v^* x^*}{U_e^*}} \int_0^\infty f_\eta(1 - f_\eta) d\eta = L_{ref}^* \sqrt{\frac{x}{ReU_e}} \int_0^\infty f_\eta(1 - f_\eta) d\eta \tag{14}$$

The friction coefficient C_f is also determined by the partial derivative $\frac{\partial u^*}{\partial y^*}$ of the wall shear stress. The local friction coefficient defined by equation is achieved by evaluating the derivative at the wall (η = 0) where U_∞^* is the free stream velocity at infinity such that

$$C_f = 2\frac{U_e^*}{U_\infty^{*\,2}} \sqrt{\frac{v^* x^*}{U_e^*}} f_{\eta\eta}(x, 0) = 2U_e \sqrt{\frac{U_e}{Rex}} f_{\eta\eta}(x, 0) \tag{15}$$

2. Methodology

2.1 Simplified Governing Equation

The Navier–Stokes equations, which are the governing equation of fluid motion is named after Claude-Louis Navier, a French engineer and physicist, and George Gabriel Stokes, an Anglo-Irish physicist and mathematician. It was difficult to solve because it was a set of nonlinear partial differential equations [1 -3]. Unlike laminar flow, which moves in smooth paths or layers, turbulent flow is characterised by irregular fluctuations or mixing. In a turbulent flow, the fluid's speed continuously changes in magnitude and direction. The two-dimensional turbulent boundary layer equation can be obtained by decomposing into a mean and fluctuating component with the assumption that the fluctuating component's mean is always zero.

We considered simplified Equation 3 to 5 of the momentum equation into an estimate of constant pressure in the normal direction when compared term by term to the x-component. Turbulent flow boundary layer equations in two dimensions are summarised as follows

$$\frac{\partial u}{\partial x}+\frac{\partial v}{\partial y}=0 \tag{16}$$

$$u\frac{\partial u}{\partial x}+v\frac{\partial u}{\partial y}=-\frac{1}{\rho}\frac{\partial \rho}{\partial x}+v\frac{\partial^2 u}{\partial y^2}-\frac{\overline{\partial u'v'}}{\partial y} \tag{17}$$

$$\frac{\partial \rho}{\partial y}=0 \tag{18}$$

2.2 Turbulence Model

In order to solve the governing equation inside the boundary layer as given by Equation 17, the Reynolds shear stress term ($\rho\frac{\overline{\partial u'v'}}{\partial y}$) has to be defined. We adopted the Cebeci-Smith Turbulence model [8, 9]. Prandtl also presented another model, which is the mixing-length notion in 1925. Despite the fact that both models were developed using incorrect physical arguments, they have proven to be extremely useful in numerous fields. Cebeci employed the Falkner-Skan variables and so the momentum equation for a turbulent flow, Equation 17, can be rewritten as

$$u\frac{\partial u}{\partial x}+v\frac{\partial u}{\partial y}=-\frac{1}{\rho}\frac{\partial \rho}{\partial x}+\frac{\partial}{\partial y}\left(b\frac{\partial u}{\partial y}\right) \tag{19}$$

where $b=v+\epsilon_m$. Thus, the addition of turbulent eddy viscosity is the only computational difference between laminar and turbulent boundary layers.

2.3 Transition point from Laminar to Turbulent Flow

In the solution of the boundary layer equations, it is necessary to predict the onset of transition and the region of transition from laminar to turbulent flow. In order to estimate the transition point, we used the Michel Method. By making use of linear stability theory and expression given in Cebeci and Smith, it suggests that transition point occurred at the point where the Reynold momentum thickness $R_{e\theta}$ and the Reynold number R_{ex} fulfil the following relation [8, 9]

$$R_{e\theta}\ \geq\ 1.174\left[1+\frac{22400}{R_{ex}}\right]{R_{ex}}^{0.46} \tag{20}$$

In above equation θ and x are the boundary layer momentum thickness and the location of control on the body surface having a distance x from the leading edge's stagnation point, respectively. The air density is ρ and μ is the air viscosity.

2.4 Numerical Techniques

2.4.1 Transformation of Airfoil Coordinates and Variables

The *x/c* and *y/c* coordinates of the airfoil were supplied as inputs and referred to as *xc* and *yc*, respectively, in the programme. Beginning at the stagnation point, the programme redefined these coordinates into a single parameter corresponding to a surface distance

$$x_i=x_{i-1}+\sqrt{(xc_i-xc_{i-1})^2+(yc_i-yc_{i-1})^2} \tag{21}$$

As a result, the variable *x* used by the programme internally in the boundary layer equations is this surface coordinate. The well known Falkner-Skan transformation was used to transform the variable *y*. Boundary layer formation was eliminated in laminar flow and reduced in turbulent flow. This increased streamwise steps while improving computational efficiency. For the *x* transformation, the reference length is the chord of an airfoil, so $\xi = x/c$. The surface distance *x* differs from the input *x/c* coordinates. Upon transformation, it produces a dimensionless stream function $f(x,\eta)$. Equation 16 and 17 and the boundary conditions may then be rewritten in terms of the new variables

$$(bf'')' + \frac{m+1}{2} ff'' + m[1-(f')^2] = \xi\left(f'\frac{\partial f'}{\partial \xi} - f''\frac{\partial f}{\partial \xi}\right)$$

$$\eta = 0 \qquad f' = 0 \qquad f(\xi,0) = f_w(\xi) = -\frac{\sqrt{R_L}}{\sqrt{\frac{u_e}{u_\infty}\xi}} \int_0^\xi \frac{v_w}{u_\infty} d\xi$$

$$\eta = \eta_e \quad f' = 1 \tag{22}$$

2.4.2 Keller's Box Method

The dimensionless stream function $f(x,\eta)$, is still in a second-order partial differential equation, hence can be numerically solved using Crank-Nicholson or Keller's box methods. The Keller's box approach begins by reformulating higher order equations into a series of first order equations. Approximation of these equations used centred-difference derivatives at each rectangular grid section. The grid points from The Keller's box method were then linearized using Newton's approach. The method assumes an approximate solution from the previous iteration cycle or streamwise station. The approximate solution was then updated with minor unknowns. A block tridiagonal matrix-vector structure allows the subroutine SOLVE in program code Keller's box method to efficiently solve for the tiny numbers. Newton's method was repeated until the small numbers were ignored [5, 7, 9].

The truncation error is of the 2nd type order. The resulting implicit nonlinear difference equations were linearized and solved by block elimination. Using the following definitions, as a first order system, the *u* and *v* in Equations 22 are not velocity components. There are two new arbitrary variable names for the first order system expression. In order to maintain consistency in the numerical explanation, these specific variable names were used. The grid points were defined as

$$\xi^n = \xi^{n-1} + k^n \qquad n = 1,2\ldots.,N \qquad \xi^0 = 0$$
$$\eta_j = \eta_{j-1} + h_n \qquad j = 1,2\ldots.,J \qquad \eta_0 = 0 \quad \eta_j = \eta_e \tag{23}$$

where *N* and *J* are the maximum number of streamwise and normal grid points used, respectively. The superscript *n*, like the subscript *j*, is a counter. This allows the use of both counts on the same variable. The box's midpoint was approximated by centering first in one direction, then the other. The boundary conditions at $\xi = \xi^0$ are

$$f_0^n = f_w \qquad u_0^n = 0 \quad u_j^n = 1 \tag{24}$$

2.5 Coordinates Files and Velocity Distribution

The airfoil geometry in this study was obtained from airfoiltools.com. In order to solve the boundary layer equation, the code demands that the velocity distribution, U_E and the number of nodes or number of panel are provided all together with the airfoil coordinates. Upon applying Bernoulli's Law for pressure, U_E can be solved for an inviscid flow. The coordinates data along the velocity distribution was arranged together in a file and saved as .dat.

3. Results and Discussion

3.1 Skin Friction Coefficient

The skin friction coefficient C_f describes the skin shear stress caused by viscous fluid flow around the airfoil's walls, and is only measured on the airfoil's suction surface.

The coefficient in boundary layer over NACA 23021 is higher than that over NACA 23012 for about 10% of the chord length from the leading edge as shown in Fig. 2. This is due to the thicker airfoil section in the case of the former. The difference in C_f is negligible for the rest of the chord length downstream.

In Fig. 3, however, C_f in boundary layer at $\alpha = 0^0$ is greater than that at $\alpha = 5^0$ for around 40% of the chord length from the leading edge. This information needs further attention, and an improvement of the prediction method is necessary. The coefficient should be greater at higher α due to the increment of wetted (or total) surface area in contact with fluids.

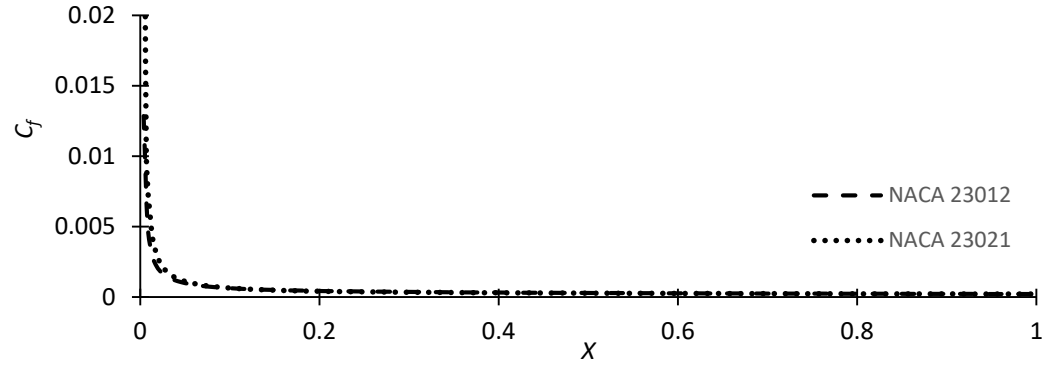

Fig. 2 – Skin Friction Coefficient of the boundary layer over NACA 23012 and NACA 23021 at $\alpha = 0^o$

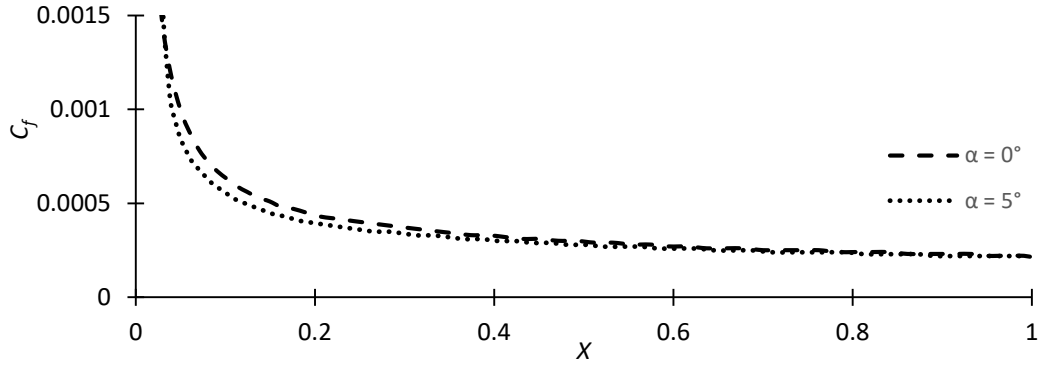

Fig. 3 – Skin friction coefficient of the boundary layer over NACA 23012 at $\alpha = 0^o$ and $\alpha = 5^o$

3.2 Momentum Thickness

When studying a boundary layer it is necessary to obtain the results of the momentum thickness δ_2^* and shape factor *H*. The shape factor is a simple parameter that relates displacement thickness δ_1^* and δ_2^*.

In general, momentum thickness of the boundary layer over NACA 23012 is higher than the boundary layer momentum thickness over NACA 23021 for the whole chord length as shown in Fig. 4. This information confirms that the lost of momentum flow rate within the boundary layer which defines δ_2^* should be higher than the rate that would occur in the case of boundary layer over thicker airfoil (i.e. NACA 23021).

The following Fig. 5 shows that δ_2^* at $\alpha = 0^o$ is bigger than δ_2^* at $\alpha = 5^o$ for approximately 30% of the chord length from the leading edge. However, the real phenomena indicate greater momentum thickness for greater α where the boundary layer tends to separate from the surface of the airfoil.

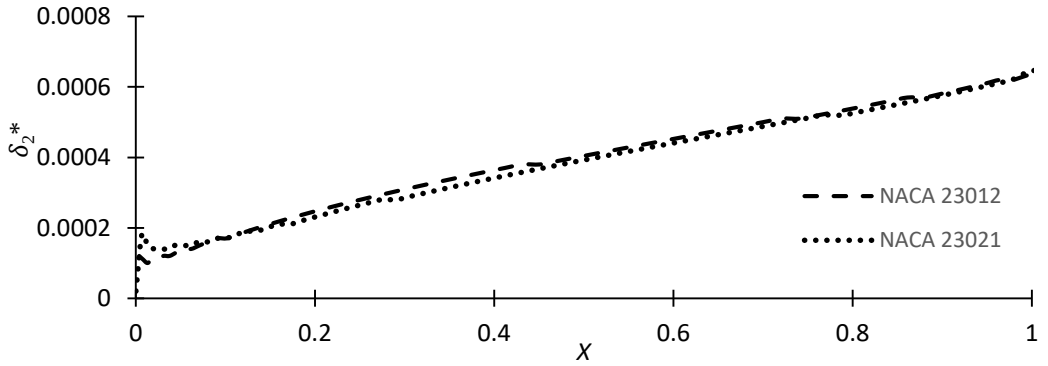

Fig. 4 – Momentum thickness of the boundary layer over NACA 23012 and NACA 23021 at $\alpha = 0^o$

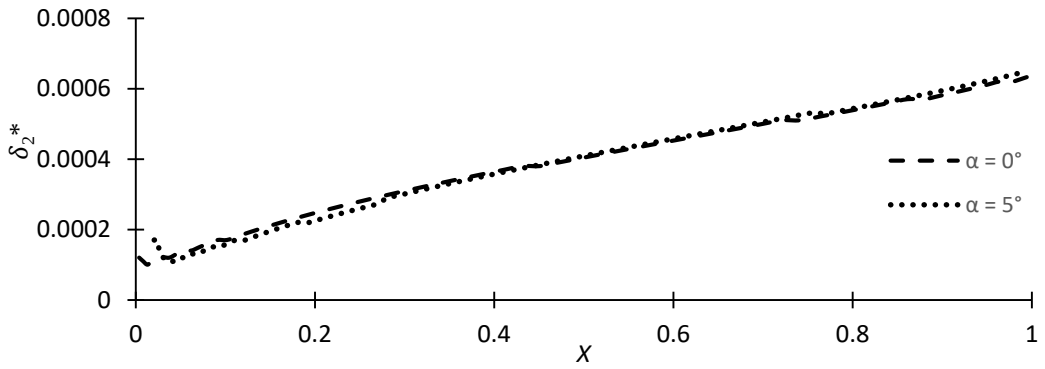

Fig. 5 – Momentum thickness of the boundary layer over NACA 23012 at $\alpha = 0^0$ and $\alpha = 5^0$

3.3 Shape Factor

In Fig. 6, the shape factor *H* for the boundary layer over NACA 23012 is bigger in comparison to NACA 23021 for about 30% of the chord length from the leading edge. This means that there is a stronger adverse pressure gradient with regard to NACA 23012. In other words, the corresponding boundary layer is relatively near separation. The difference in *H* is negligible for the rest of the chord length downstream.

In Fig. 7, *H* at $\alpha = 0^0$ is greater in comparison to $\alpha = 5^0$, in general. Obviously, the prediction method needs to be enhanced for a better illustration. The factor should be greater at higher α indicating the bigger possibility for boundary layer separation.

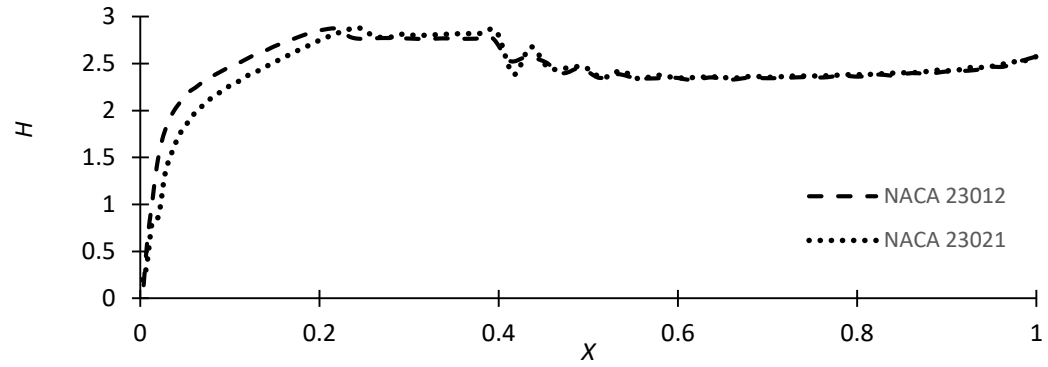

Fig. 6 – Shape factor of the boundary layer over NACA 23012 and NACA 23021 at $\alpha = 0^0$

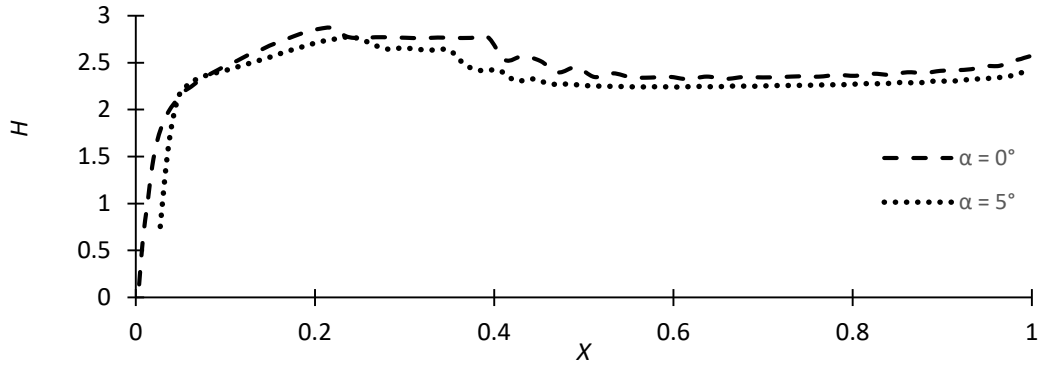

Fig. 7 - Shape factor of the boundary layer over NACA 23012 at $\alpha = 0^0$ and $\alpha = 5^0$

3.4 Average Difference

Comparative parameter profiles given in Fig. 2 to Fig. 7 were reconfirmed by calculating average difference between data values (i.e. those of C_f, δ_2*, and H) with respect to airfoils as well as angles of attack α. The corresponding values are listed in Table 1 and Table 2. We take NACA 23012 and $\alpha = 0^o$ as references.

Table 1 - Average difference between the parameters of boundary layer over NACA 23012 and NACA 23021 at $\alpha = 0^o$

Parameter	Average Difference	
C_f	$C_{f\,23021}$-$C_{f\,23012}$	= 1.3 x 10^{-03}
δ_2*	θ_{23021}-θ_{23012}	= -2.3 x 10^{-06}
H	H_{23021}-H_{23012}	= -4.6 x 10^{-02}

Table 2 - Average difference between the parameters of boundary layer over NACA 23012 at $\alpha = 0^o$ and $\alpha = 5^o$

Parameter	Average Difference	
C_f	$C_{f\,5}$-$C_{f\,0}$	= -1.5 x 10^{-04}
θ	θ_5-θ_0	= -1.7 x 10^{-05}
H	H_5-H_0	= -1.1 x 10^{-01}

4. Conclusion

This paper highlights the study of boundary layer over airfoils NACA 23012 and NACA 23021. This aids in comparative understanding on flow behaviors between airfoils as well as angles of attack. Three major parameters of interest, namely skin friction factor C_f, momentum thickness, δ_2* and shape factor H, were successfully generated with respect to x. It also shares some useful research data on overall airfoil performance by investigating changes in boundary layer characteristics. The programme code used is particularly unique, and proven to be beneficial in achieving the objectives of study. Future study would involve the location of transition between laminar and turbulent flow in boundary layer, and the flow separation.

Acknowledgement

The author would like to thank Universiti Tun Hussein Onn Malaysia (UTHM) and Ministry of Higher Education of Malaysia (MoHE) for the research facilities.

References

[1] H. Schlichting , and K. Gersten, “Boundary layer theory,” 8th edition, Berlin, Germany: Springer, 2000.
[2] T. Cebeci, and P. Bradshaw, “Momentum transfer in boundary layers,” Washington, 1977.
[3] J. D Anderson, "Ludwig Prandtl’s boundary layer.," *Physics Today*, vol. 58, pp. 42-48, 2005.
[4] K. Pohlhausen, "Zur näherungsweisen integration der differentialgleichung der laminaren grenzschicht.," *Journal of Applied Mathematics and Mechanics*, vol. 1, no. 4, pp. 252-290, 1921.
[5] T. A. J. Cousteix, “Modeling and computation of boundary-layer flows,” 2nd Edition, Berlin, Germany: Springer, 2005.
[6] J. Moran, “An introduction to theoretical and computational aerodynamics,” New York: John Wiley, 1984.
[7] T. J Chung, “Computational fluid dynamics,” Cambridge University Press, 2nd Edition, 2002.
[8] T. Cebeci, “Turbulence models and their application,” California: Horizonz Publishing, 2004.
[9] T. C. A. Smith, “Computation of turbulent boundary layers,” California: Stanford University Press, 1968.